engineering proceedings

MDPI

Proceeding Paper

Performance Analysis and Resilience Assessment of a Hybrid PV–Wind Integrated 9-Bus Power System †

Senthil Krishnamurthy * and Abuyile Mpaka

Center for Intelligent Systems and Emerging Technologies, Department of Electrical, Electronic, and Computer Engineering, Cape Peninsula University of Technology, Bellville, Cape Town 7535, South Africa; ampaka4@gmail.com

* Correspondence: krishnamurthys@cput.ac.za; Tel.: +27-(0)-21-959-5818

† Presented at the 34th Southern African Universities Power Engineering Conference (SAUPEC 2026), Durban, South Africa, 30 June–1 July 2026.

Abstract

The addition of renewable energy sources (RES), including photovoltaic (PV) and wind generation technology, has introduced new challenges and opportunities for modern power systems. This paper examines the functionality and reliability of a hybrid PV—wind-integrated 9-bus power system evaluated in DIgSILENT PowerFactory. The system has been designed with two solar PV plants, two offshore wind farms, multiple loads, and transformer interconnections, and aims to evaluate steady-state, dynamic, and contingency behavior. The system was evaluated using load-flow, quasi-dynamic, and RMS simulations to assess power balance, voltage stability, and fault recovery. The outcomes indicated convergence, balanced power flow, and system resilience under single-contingency conditions. This paper shows the effectiveness of the power system simulation tool for analyzing hybrid renewable power systems.

Keywords: hybrid power system; photovoltaic; wind energy; load flow; quasi-dynamic simulation; contingency analysis; DigSILENT PowerFactory

1. Introduction

The global energy transition has led to the extensive integration of renewables, primarily solar PV and wind, into modern power networks. These distributed, meshed systems enable decarbonisation while also being much more reliable and resilient. Their intermittent and variable nature, however, presents challenges for voltage stability, harmonic distortion, and frequency control [1–3]. The hybrid PV–wind system improves reliability by providing a complete solution to solar and wind intermittencies [4,5]. Analyzing the integration of renewable energy and its consequent ramifications on the power system has increased the use of power system modeling frameworks, such as DIgSILENT PowerFactory Version 2025. Renewable sources modeling for harmonic assessment was investigated in [6,7]. PV models in DIgSILENT grids were tested for predictive precision in the Malaysian grid models' dynamic performance [8] for large-scale PV system integration, with focus on South African grid codes and LVRT, as well as reactive power control. Further to this, [9] and other authors [10,11] emphasized the importance of grid-support functionalities that are essential for maintaining voltage control and dynamic rate. Numerous investigations have been conducted on hybrid system optimization and control strategies [12], recommending hybrid control strategies for coordinated control of hybrid PV–wind systems. Ref. [13] studied the multi-objective optimization problem for grid-tied renewable systems, and [14,15]

Check for updates

Academic Editor: Akshay Kumar Saha

Published: 12 May 2026

Copyright: © 2026 by the authors. Licensee MDPI, Basel, Switzerland. This article is an open access article distributed under the terms and conditions of the Creative Commons Attribution (CC BY) license.

worked on the hybrid RES in microgrid applications to improve microgrid reliability and cost-effectiveness. Also, adaptive algorithms such as fuzzy logic and model predictive control have been employed to address voltage stability during weather changes [16,17].

In the resilience assessment, hybrid systems must cope with grid faults, adapt to changes in renewable energy sources, and handle load fluctuations. The resilience metrics introduced in [18] and further developed in [19] enable a systematic analysis of a system's recovery and robustness over extended periods of operation without external support. Multiple contributions have been made to studies on renewable integration in classical benchmark networks, such as the IEEE 9-bus system. The most recent, presented at the IEEE Global Energy Conference 2024, explores load flow and fault studies in renewable-penetrated systems. Previous studies have also explored modeling of renewables, harmonics, and grid code compliance using DIgSILENT PowerFactory tools. While it provides information on steady-state and transient phenomena, this previous work on the IEEE 9-bus network focuses primarily on operational feasibility rather than on quantifiable aspects of resilience [20].

This paper is structured in the following way. Section 2 covers the hybrid PV–wind system and its modeling approach, and explains the design calculations that set the system parameters. The load flow analysis, quasi-dynamic, and RMS simulations to evaluate the system's time-dependent behavior are performed in Section 3, and assessed for resilience under contingency scenarios in Section 4. Finally, Section 5 concludes the paper by presenting the conclusions and outlining the main outcomes and their industry relevance.

2. System Description and Modeling

The designed system includes nine buses connected via four transmission lines, two PV plants (8 MW and 18 MW), two wind turbines (40 MW and 20 MW), three loads, and five transformers. This model was built in DigSilent PowerFactory (DPF), as shown in Figure 1.

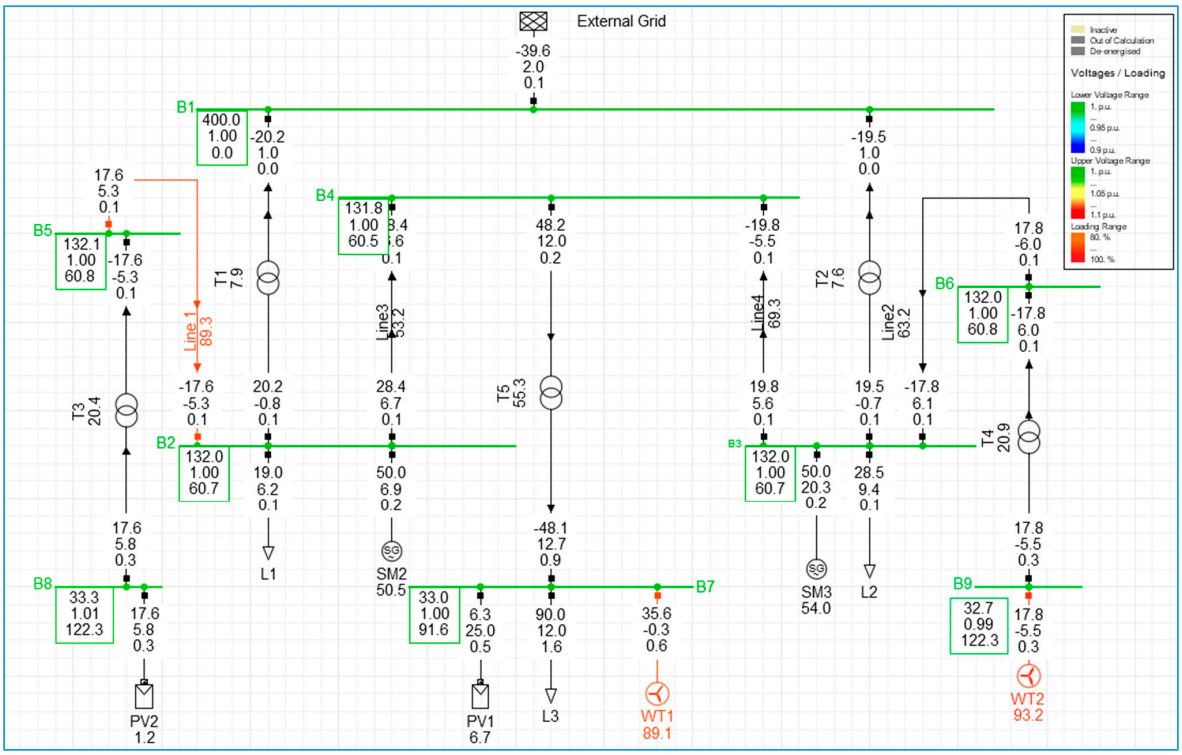


Figure 1. Single-line diagram of the 9-bus power system network.

Design Calculations

The design comprises an 18 MW photovoltaic (PV) plant and two wind turbine (WT) farms, 40 MW (WT1) and 20 MW (WT2), for a total of 60 MW. The design considers global best practices for large-scale renewable integration, including optimized sizing, energy yield calculations, and design reliability.

A. **PV2 Plant Design for 18 MW**

The design of the 18 MW solar PV plant entails determining the most economically viable configuration for the required number of photovoltaic modules, inverter sizing, and the DC-to-AC ratio to achieve optimal plant performance and system efficiency.

(1) **Determination of PV Modules**

The calculations below are for Equation (1), assuming an individual PV module rated at 400 W (0.4 kW). This means the total number of modules N_{PV} needed for an 18 MW (18,000 kW) installation is given by the following equation:

$$N_{PV} = \frac{P_{total}}{P_{panel}} = \frac{18,000\ \text{kW}}{\frac{0.4\ \text{kW}}{panel}} = 45,000\ panels \quad (1)$$

(2) **Inverter Sizing**

String inverters are modular and dependable, which is why they are popular in utility-scale systems. Each inverter has a nominal capacity of 250 kW, and the number of inverters N_{inv} required is:

$$N_{inv} = \frac{P_{total}}{P_{inv}} = \frac{18,000\ \text{kW}}{\frac{250\ \text{kW}}{inverter}} = 72\ inverters \quad (2)$$

(3) **DC-to-AC Ratio**

To account for irradiance fluctuations, temperature effects, and inverter efficiency, an over-sizing ratio of 1.1–1.25 is typically applied. Contemplating a ratio of 1.2, the effective DC capacity per inverter is:

$$P_{DC} = P_{inv} \times 1.2 = 250\ \text{kW} \times 1.2 = 300\ \text{kW} \quad (3)$$

Therefore, the number of panels per inverter is:

$$N_{\frac{PV}{inv}} = \frac{P_{DC}}{P_{panel}} = \frac{300,000\ \text{W}}{400\frac{\text{W}}{panel}} = 750\frac{panels}{inverter} \quad (4)$$

This configuration optimizes DC bus utilization and enables it to serve multiple functions under varying solar conditions.

B. **Wind Turbine WT1 Design (40 MW)**

At first wind installation (WT1), each turbine is rated at 2 MW. The power curve model presents the correlation between wind speed, V, and power output $P(V)$. There are three operational power generation regions:

- Region 1: $V < V_{cut-in}$—No power generation;
- Region 2: $V_{cut-in} \leq V < V_{rated}$—Power increases polynomials with wind speed;
- Region 3: $V_{rated} \leq V < V_{cut-out}$—Constant power at rated capacity.

https://doi.org/10.3390/engproc2026140005

The power output model is presented as:

$$P(V) = \begin{cases} 0, & if\ V < V_{cut-in} \\ P_{rated}\left(\frac{V - V_{cut-in}}{V_{rated} - V_{cut-in}}\right)^k & if\ V_{cut-in} \leq V < V_{rated} \\ P_{rated,} & if\ V_{rated} \leq V < V_{cut-out} \end{cases} \quad (5)$$

where

- P_{rated} = Rated power output;
- V_{cut-in} = Cut-in wind speed;
- V_{rated} = Rated wind speed;
- $V_{cut-out}$ = Cut-out wind speed;
- k = Exponent determining the shape of the curve.

$$P_{rated} = 2\ \text{MW},\ V_{cut-in} = 3\frac{m}{s},\ V_{rated} = 12\ \text{m/s},\ V_{cut-out} = 25\frac{m}{s}, \text{and } k = 3.$$

To attain a total installed capacity of 40 MW, the essential number of turbines is:

$$N_{WT1} = \frac{P_{total}}{P_{rated}} = \frac{40\ \text{MW}}{2\frac{\text{MW}}{turbine}} = 20\ turbines \quad (6)$$

By applying the above power curve function across varying wind speeds, the aggregated wind farm generation profile can be estimated to evaluate the capacity factor and annual energy yield.

C. Wind Turbine WT2 Design (20 MW)

For the secondary wind installation (WT2), identical turbine specifications are assumed to ensure model uniformity and simplify maintenance. The total quantity of turbines required for a 20 MW configuration is:

$$N_{WT2} = \frac{P_{total}}{P_{rated}} = \frac{20\ MW}{2\frac{MW}{turbine}} = 10\ turbines \quad (7)$$

The same analytical model used for WT1 is applied to WT2, enabling integration of both subsystems into the 9-bus architecture for collective performance and reliability evaluation.

D. Wind Turbine Power Curve Data and Validation

Initially, we needed to assess WT1's power output across different wind speeds to characterize its performance. Wind-power characteristics are summarized in Table 1. This shows the typical power output nonlinearity as a turbine progresses from cut-in to rated operation. From the discrete wind speeds and the electrical power generated at those speeds, the turbine's power curve was created. This serves as validation of the WT1 model's behavior, which we will compare with the empirical datasets later in the text.

https://doi.org/10.3390/engproc2026140005

Table 1. WT1 power curve: wind speed vs. electrical power output.

Wind Speed m/s	Power in MW
4.435	0.152398
7.615	0.812386
10.308	1.511297
11.487	1.718976
11.815	1.762164
12.107	1.797685
12.549	1.844666
12.56	1.839808
12.709	1.748383

We used operational data from the [20] platform to improve the simulated turbines' features. As shown in Table 2, the dataset includes synchronized time series data with UTC and local timestamps, recorded wind speeds, and power output for a comparable wind-energy facility, as well as datasets with spatial timestamps and wind/power output for a comparable wind-energy facility. This dataset illustrates two aspects: the alignment between the simulated WT1 power curve and field performance, and the validation of the wind-speed selection for subsequent RMS and contingency simulations.

Table 2. Empirical wind-speed and power production data obtained from [20].

# {"Units": {"Time": "UTC"	"Local_Time": "Africa/Johannesburg"	Electricity kW	Wind Speed m/s
2 January 2019 16:00	2 January 2019 18:00	152.398	4.435
2 January 2019 17:00	2 January 2019 19:00	812.386	7.615
2 January 2019 18:00	2 January 2019 20:00	1511.297	10.308
2 January 2019 19:00	2 January 2019 21:00	1718.976	11.487
2 January 2019 20:00	2 January 2019 22:00	1762.164	11.815
2 January 2019 21:00	2 January 2019 23:00	1797.685	12.107
2 January 2019 22:00	3 January 2019 00:00	1844.666	12.549
2 January 2019 23:00	3 January 2019 01:00	1839.808	12.56
3 January 2019 00:00	3 January 2019 02:00	1748.383	12.709

E. Summary of Design Parameters

Component Rated Power Unit Rating Quantity Remarks PV2 Plant 18 MW 400 W/panel 45,000 panels 72 inverters (250 kW each) WT1 Farm 40 MW 2 MW/turbine 20 turbines modeled with a cubic power curve WT2 Farm 20 MW 2 MW/turbine 10 turbines, a similar configuration to WT1. This configuration facilitates balanced hybrid operation within the IEEE 9-bus network, verifying adequate reactive support, harmonic compliance, and resilience against wind and solar variability.

3. Load Flow, Quasi-Dynamic, and RMS Simulations

Load flow simulations confirmed balanced operation with total generation and load power nearly equal, indicating negligible losses and stable voltage profiles across all buses. The load flow summary is provided in Table 3.

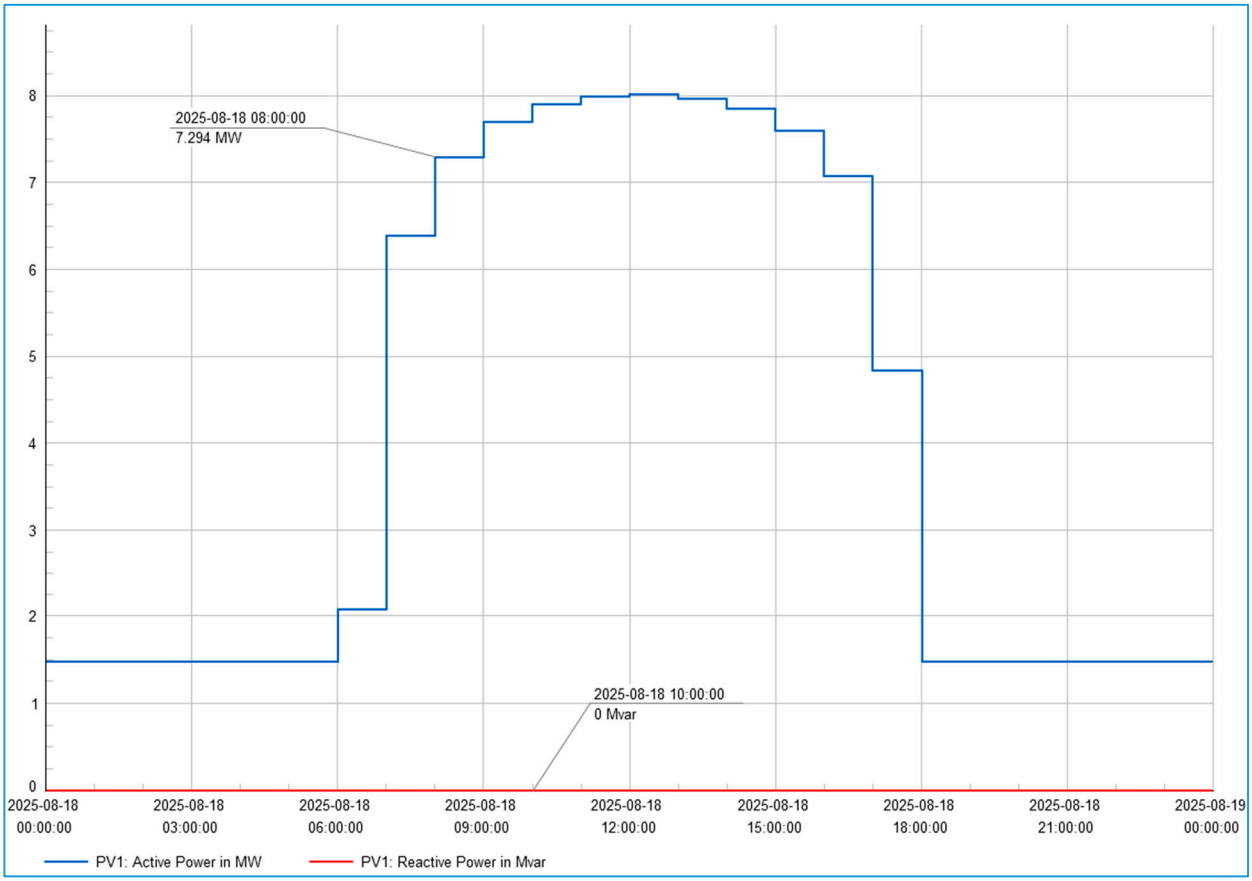
Table 3. Load flow summary.

Source	P (MW)	Q (MVar)	I (kA)
Grid	−11.4	0.5	0.016
SM2	40	11.8	0.182
SM3	11.7	28.2	0.100
WT1	35.6	−0.3	0.800
WT2	17.8	−5.5	0.300
PV1	6.3	2.1	0.100
PV2	17.6	5.8	0.300

3.1. Quasi-Dynamic Simulation of PV1 Plant

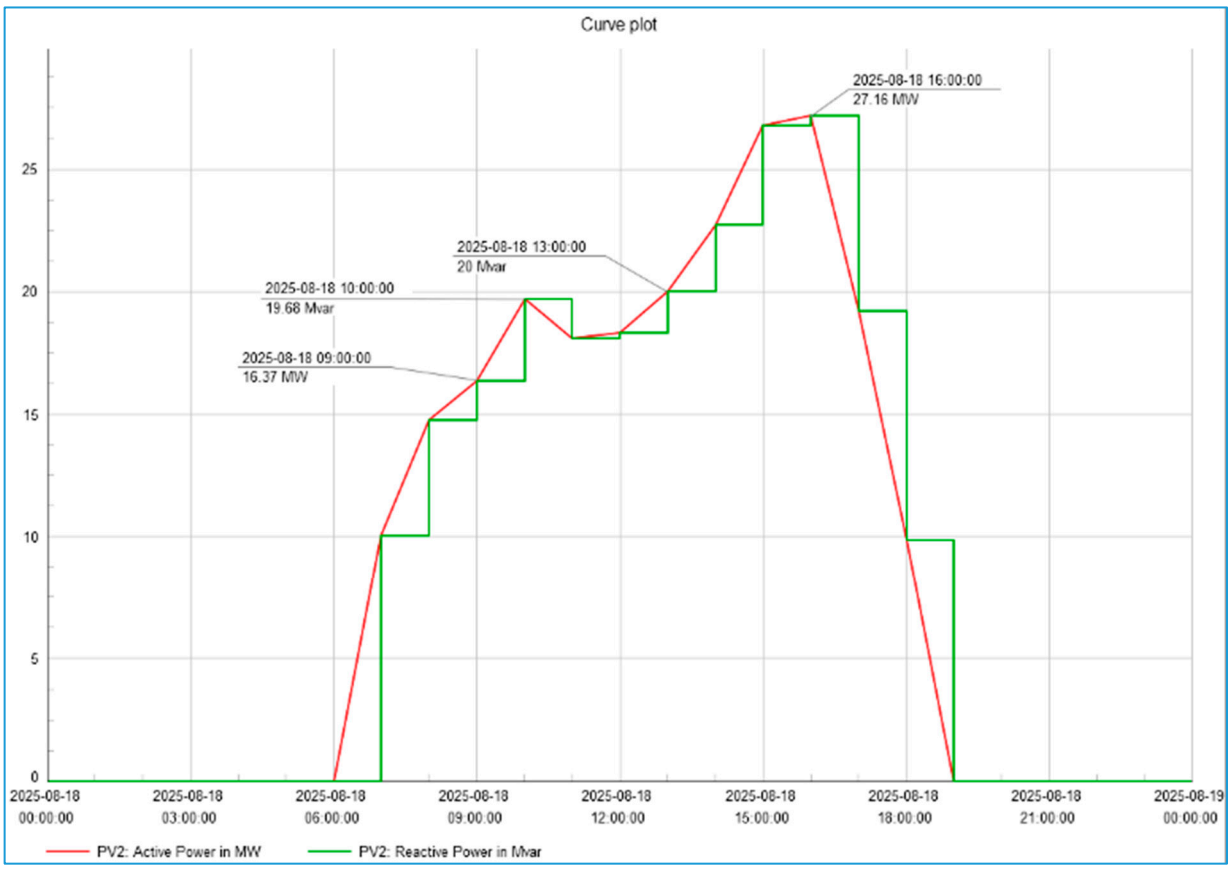
The quasi-dynamic simulation output for the PV plant was as expected for daytime generation. In the 3 s RMS simulations, the influence of varying wind speeds in all three areas also confirmed system stability and grid control.

A 24 h quasi-dynamic simulation run on 18 August 2025 assessed the PV1 plant's real and reactive power outputs. The active power output showed expected daytime behavior, peaking at 7.294 MW at 08:00 before falling with solar irradiance. The reactive power output remained at 0 Mvar, confirming unity power factor operation and effective voltage control. As shown in Figure 2a, these results confirm daytime operation and successful inverter–grid interaction in normal conditions.



(**a**) Quasi-dynamic simulation of PV Plant 1

Figure 2. *Cont.*



(**b**) Quasi-dynamic simulation of PV Plant 2

Figure 2. Active and reactive power profiles during the 24 h quasi-dynamic simulation. (**a**) PV Plant 1 and (**b**) PV Plant 2.

3.2. Quasi-Dynamic Simulation of PV2 Plant

A continuous quasi-dynamic simulation for 24 h on the PV2 plant. Figure 2b active power (in red) increases with solar irradiance till it peaks at 27.14 MW at 16:00 before decreasing again toward sunset. As for reactive power (in green), it follows the inverter control steps to support voltage. The results certify an efficient and PV2-stable response to daily solar variation.

4. Contingency Analysis

A single outage-related contingency of wind turbine 2 (17.8 MW) was simulated. The grid transitioned from absorbing −11.4 MW to supplying 6.4 MW to maintain load balance. This presented the system's resilience in the face of generator loss, as shown in Figure 3.

The network resilience test was conducted by applying a single contingency to Wind Turbine 2 (WT2), and the disturbance and recovery. The change in real power output due to contingency was transferred to the coupled buses and other generators. Monitoring WT2 control actions in this case supports its ability to quickly regulate them, dampen oscillations, restore voltage, and return the active power output to its original value. These results confirm the grid's dynamical resilience and WT2's sensitivity to changes in network topology.

https://doi.org/10.3390/engproc2026140005

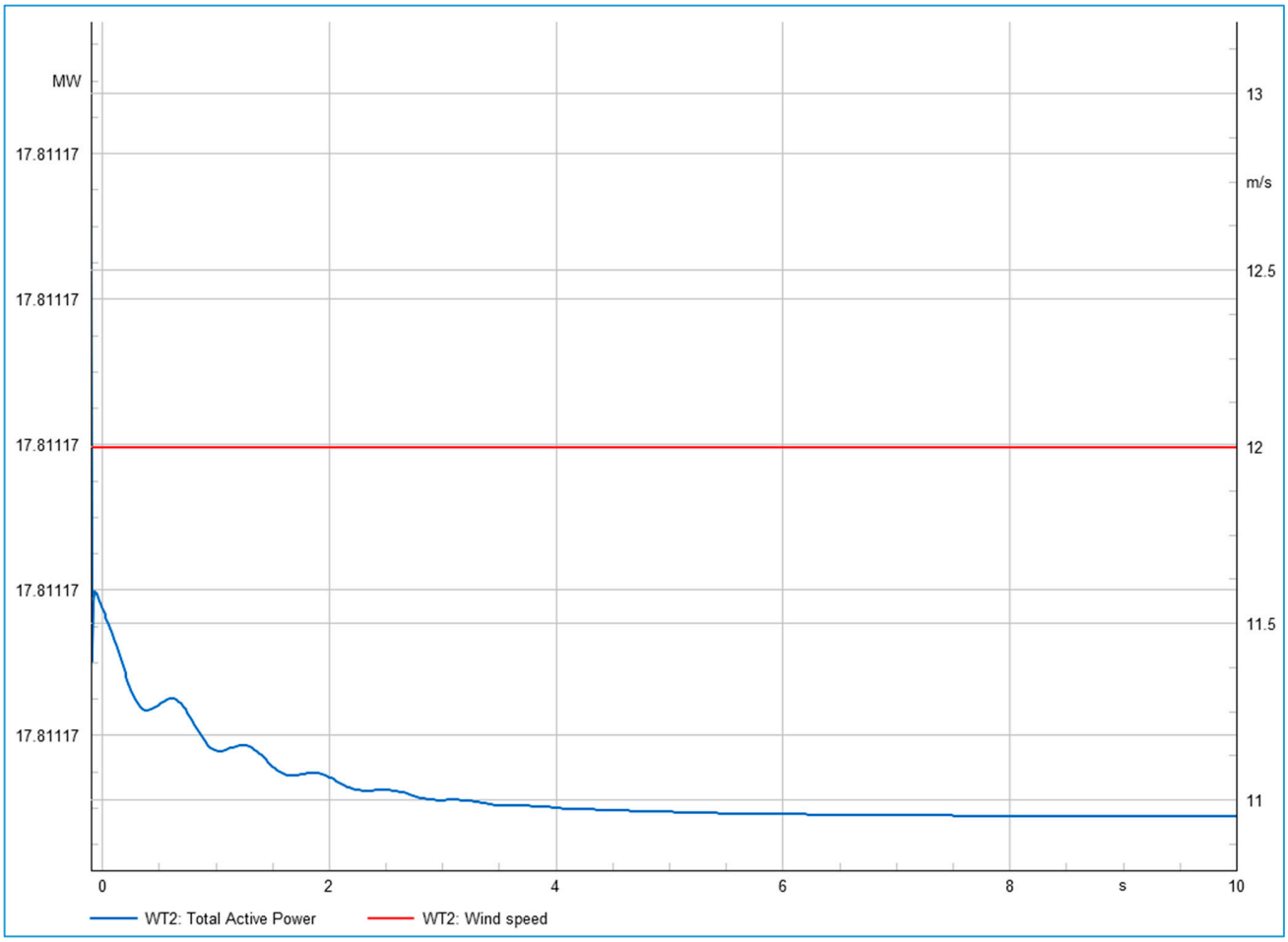


Figure 3. The real power and wind speed of the WT2 Plant for 3 s.

The impact of the WT2 outage on power flows with the external grid is shown in Table 4 for the normal and contingency cases. The normal case has an export of −39.6 MW, reflecting the surplus generation from the IPPs. Generation decreases by 17.8 MW due to WT2 losses, reducing net exports. This aligns with the adjusted export of around −21.7 MW (−39.5 + 17.8), as evidenced by the −21.9 MW value in Table 4, illustrating the grid's adjustment to fluctuations in renewable generation.

Table 4. Overview of power transfer under normal and contingency conditions.

Operating Condition	Power (MW)	Description
Normal operation (no contingency)	−39.6	Net power exported to the external grid due to surplus IPP generation
WT2 out of service (contingency condition)	17.8	Power lost due to WT2 generation being unavailable
Resulting net export after WT2 contingency	−21.9	Reduced export to the grid (≈−39.5 + 17.8 = −21.7 MW)

5. Conclusions

The effectiveness and resilience of a hybrid PV–wind integrated 9-bus power system were analyzed in this paper using DIgSILENT PowerFactory. Evaluated results indicate that coordinated integration of solar and wind generation improves system reliability by enhancing voltage stability. Furthermore, the hybrid system design minimizes intermittency, resulting in smoother power output and strengthened grid performance. Reliability

assessment of the system further illustrates the enhanced effectiveness of its recovery and disturbance performance relative to the strength of single-source renewables. This emphasizes the hybrid's unique potential. The integration of renewables results in controlled hybrid systems that significantly improve grid performance and voltage regulation. Advanced optimization, paired with energy storage, will provide the grid ancillary support and operational resilience to enable essential smart grid applications.

Author Contributions: S.K.: conceptualization, methodology, software, validation, A.M. and S.K.: formal analysis, investigation, S.K.: resources, data, editing, supervision, visualization, project administration, funding acquisition. A.M. and S.K.: writing, reviewing, and editing. All authors have read and agreed to the published version of the manuscript.

Funding: This work was supported in part by the National Research Foundation (NRF), under Thuthuka Grant 138177, in part by the Eskom Tertiary Education Support Program (TESP) through a research grant, and in part by the Eskom Power Plant Engineering Institute (EPPEI), French Embassy AI-Furgal Grant 2025-135.

Institutional Review Board Statement: Not applicable.

Informed Consent Statement: Not applicable.

Data Availability Statement: Data are contained within the article.

Acknowledgments: The researchers acknowledge the support and assistance of the Center for Intelligent Systems and Emerging Technologies in the Department of Electrical, Electronic, and Computer Engineering at Cape Peninsula University of Technology, Bellville, Cape Town 7535, South Africa, for their financial and material support in executing this research project. The opinions presented in this paper are those of the authors and not the funders.

Conflicts of Interest: The authors declare no conflicts of interest.

References

1. Wen, L.; Zhou, K.; Feng, W.; Yang, S. Demand Side Management in Smart Grid: A Dynamic-Price-Based Demand Response Model. *IEEE Trans. Eng. Manag.* **2024**, *71*, 1439–1451. [CrossRef]
2. Alhelou, H.H.; Hamedani-Golshan, M.E.; Njenda, T.C.; Siano, P. Wide-area measurement system-based optimal multi-stage under-frequency load-shedding in interconnected smart power systems using evolutionary computing techniques. *Appl. Sci.* **2019**, *9*, 508. [CrossRef]
3. Gautam, D.; Vittal, V.; Harbour, T. Impact of increased penetration of DFIG-based wind turbine generators on transient and small signal stability of power systems. *IEEE Trans. Power Syst.* **2009**, *24*, 1426–1434. [CrossRef]
4. Sinha, S.; Chandel, S.S. Review of recent trends in optimization techniques for solar photovoltaic wind-based hybrid energy systems. *J. Renew. Sustain. Energy Rev.* **2015**, *50*, 755–769. [CrossRef]
5. Deng, Z.; Todeschini, G.; Koo, K.L.; Mulimakwenda, M. Modelling renewable energy sources for harmonic assessments in digsilent powerfactory: Comparison of different approaches. In *Proceedings of the 11th International Conference on Simulation and Modeling Methodologies, Technologies and Applications, SIMULTECH 2021*; SciTePress: Setúbal, Portugal, 2021; pp. 130–140. [CrossRef]
6. Perumal, P.; Ramasamy, A.K.; Teng, A.M. Performance Analysis of the DigSILENT PV Model Connected to a Modelled Malaysian Distribution Network. *Int. J. Control Autom.* **2016**, *9*, 75–88. [CrossRef]
7. Sagonda, A.F.; Ainah, P.K. Grid Integration of Utility Scale Photovoltaic (PV) Plants Under the South African Grid Code Using a Modified Generic PV Model in DigSilent. *Int. J. Mechatron. Electr. Comput. Technol. (IJMEC)* **2021**, *11*, 4843–4851.
8. Ali, M.A.S.; Mehmood, K.K.; Baloch, S.; Kim, C.H. Modified rotor-side converter control design for improving the LVRT capability of a DFIG-based WECS. *Electr. Power Syst. Res.* **2020**, *186*, 106403. [CrossRef]
9. Blaabjerg, F.; Chen, Z.; Kjaer, S.B. Power electronics as efficient interface in dispersed power generation systems. *IEEE Trans. Power Electron.* **2004**, *19*, 1184–1194. [CrossRef]
10. Charalambous, A.; Hadjidemetriou, L.; Kyriakides, E.; Polycarpou, M.M. A Coordinated Voltage-Frequency Support Scheme for Storage Systems Connected to Distribution Grids. *IEEE Trans. Power Electron.* **2021**, *36*, 8464–8475. [CrossRef]
11. Kong, L.; Cai, G.; Xue, S.; Li, S. Modeling and coordinated control strategy of large-scale grid-connected wind/photovoltaic/energy storage hybrid energy conversion system. *Math. Probl. Eng.* **2015**, *2015*, 682321. [CrossRef]

12. Barakat, S.; Ibrahim, H.; Elbaset, A.A. Multi-objective optimization of grid-connected PV-wind hybrid system considering reliability, cost, and environmental aspects. *Sustain. Cities Soc.* **2020**, *60*, 102178. [CrossRef]
13. Al-Quraan, A.; Al-Qaisi, M. Modelling, design and control of a standalone hybrid PV-wind micro-grid system. *Energies* **2021**, *14*, 4849. [CrossRef]
14. Pouryekta, A.; Ramachandaramurthy, V.; Mithulananthan, N.; Arulampalam, A. Islanding Detection and Enhancement of Microgrid Performance. *IEEE Syst. J.* **2018**, *12*, 3131–3141. [CrossRef]
15. Meng, L.; Sanseverino, E.R.; Luna, A.; Dragicevic, T.; Vasquez, J.C.; Guerrero, J.M. Microgrid Supervisory Controllers and Energy Management Systems: A Literature Review. *Renew. Sustain. Energy Rev.* **2016**, *60*, 1263–1273. [CrossRef]
16. Li, S.; Oshnoei, A.; Blaabjerg, F.; Anvari-Moghaddam, A. Hierarchical Control for Microgrids: A Survey on Classical and Machine Learning-Based Methods. *Sustainability* **2023**, *15*, 8952. [CrossRef]
17. Panteli, M.; Mancarella, P. Modeling and evaluating the resilience of critical electrical power infrastructure to extreme weather events. *IEEE Syst. J.* **2017**, *11*, 1733–1742. [CrossRef]
18. Zhang, H.; Wang, P.; Yao, S.; Liu, X.; Zhao, T. Resilience Assessment of Interdependent Energy Systems under Hurricanes. *IEEE Trans. Power Syst.* **2020**, *35*, 3682–3694. [CrossRef]
19. Saha, S.; Alam, F.; Sayada, R.; Rahman, R.M.; Hasan, A.S.M.J. Advanced Load Flow & Fault Analysis of Renewable Energy Integration in IEEE 9 Bus Power System. In *IEEE Global Energy Conference 2024, GEC 2024*; IEEE: New York, NY, USA, 2024; pp. 338–347. [CrossRef]
20. Renewables.ninja. Available online: https://www.renewables.ninja/ (accessed on 30 January 2025).

Disclaimer/Publisher's Note: The statements, opinions and data contained in all publications are solely those of the individual author(s) and contributor(s) and not of MDPI and/or the editor(s). MDPI and/or the editor(s) disclaim responsibility for any injury to people or property resulting from any ideas, methods, instructions or products referred to in the content.